Mineral Dissolution and the Evolution of k_0

Hosung Shin[1] and J. Carlos Santamarina[2]

Abstract: Adequate knowledge of the in situ state of stress can be essential to the analysis of geotechnical systems. However, the measurement and prediction of k_0 remain difficult. In particular, limited attention has been given to the evolution of k_0 during the formation history of the soil and diagenetic processes such as mineral dissolution. Experimental and numerical results show that grain mass loss due to mineral dissolution produces a pronounced horizontal stress drop under zero lateral strain conditions; the state of stress may reach the active shear failure k_a condition and internal shear planes may develop. While horizontal stress recovery often follows upon further dissolution, marked differences in fabric are observed between the pre and postdissolution soil structures.

CE Database subject headings: Soil structures; Stress; Minerals.

Introduction—Previous Studies

The current stress level in the ground has important effects on the load-deformation response of soils and the performance of engineered geosystems. Hence, the stress ratio k_0 between the horizontal and the vertical effective stresses under zero lateral strain conditions is an important parameter in analysis and design.

The value of k_0 reflects soil characteristics and stress history. Theoretical and empirical relationships have been proposed to estimate k_0. Jaky's equation is widely used for nonpreloaded sediments (Jaky 1944; Michalowski 2005)

$$k_{0\langle NC \rangle} = 1 - \sin(\phi) \quad NC = \text{not preloaded} \tag{1}$$

where ϕ=constant volume friction angle. Jaky's expression does not invoke stress level (explicitly) in agreement with experimental observations in the absence of grain crushing or contact creep [Note: higher k_0 values are observed in looser soils—Bishop and Eldin (1953); Andrawes and El-Sohby (1973)]. It is interesting to note that k_0 is a function of the frictional resistance of the soil, even though the state of stress is away from the failure state (Feda 1984; Michalowski 2005). This being said, the decrease in k_0 with increasing friction angle captured in Jaky's equation is consistent with the asymptotic value $k_0=1.0$ for $\phi=0$, i.e., the hydrostatic state in fluids (Mesri and Hayat 1993), and compatible with equivalent continuum models such as the modified cam clay that take compressibility into consideration (Roscoe and Burland 1968; see discussion in Muir Wood 1990).

The preloading of frictional granular material leaves residual horizontal stresses locked in. Therefore, the prediction of k_0 during unloading must take into consideration the preload ratio or overconsolidation ratio (OCR)

$$k_{0\langle OC \rangle} = k_{0\langle NC \rangle} \text{OCR}^m \quad OC = \text{preloaded} \tag{2}$$

where the at-rest rebound parameter of the soil m is often related to friction, e.g., $m = \sin(\phi)$ (Mayne and Kulhawy 1982).

In uncemented soils, the lower limit for $k=$active stress coefficient k_a, and the upper limit is the passive stress coefficient k_p (Abdelhamid and Krizek 1976; Brooker and Ireland 1965; Feda 1984; Mayne and Kulhawy 1982); for example, k_0 in preloaded London clay approaches k_p (Mayne and Kulhawy 1982; Skempton 1961).

The value of k_0 increases with increasing plasticity in nonpreloaded fine-grained soils (Brooker and Ireland 1965), but the trend may be very weak (Kulhawy and Mayne 1990); different fabrics and pore solution have a secondary effect (Abdelhamid and Krizek 1976). The evolution of k_0 during secondary compression under no lateral strain is controversial. A decrease in k_0 could be expected due to the increase in strength with aging (see discussion in Schmertmann 1983). On the other hand, theoretical creep analyses and limited experimental data predict an increase in k_0 in nonpreloaded soils, approaching $k_0 \approx 1.0$ with time (Kavazanjian and Mitchell 1984), yet, there are other experimental results that show a seemingly constant value of k_0 during secondary compression (Holtz and Jamiolkowski 1985; Jamiolkowski et al. 1985).

Limited data are available for the evolution of k_0 during drying (Slatter et al. 2005). The value of k_0 remains constant before air entry (lateral boundary conditions must be corrected or compensated for suction—required when interpreting Slatter et al. 2005 data). Once suction exceeds the air entry value, the total horizontal stress decreases as suction continues to increase; the evaluation of k_0 in this region is conditioned by the definition of effective stress. The evolution of k_0 during cementation depends on the contractive strain the cementing agent may impose on the granular matrix. If the soil is cemented at low effective confinement $\sigma_z' = \alpha$, further zero-lateral-strain loading to $\sigma_z' = \beta > \alpha$ takes place at a very low k_0 value (even lower than k_a for the uncemented sediments) (Berre et al. 1995; Zhu et al. 1995). Finally, if the cement is dissolved while the applied vertical effective stress is maintained at $\sigma_z' = \beta$, the value of k_0 will increase toward the k_0

[1]Graduate Student, School of Civil and Environmental Engineering, Georgia Institute of Technology, Atlanta, GA 30332 (corresponding author). E-mail: hosung.shin@gatech.edu
[2]Professor, School of Civil and Environmental Engineering, Georgia Institute of Technology, Atlanta, GA 30332.

value that corresponds to the uncemented soil (Castellanza and Nova 2004).

There is no information on the evolution of k_0 in soils that have experienced postdepositional grain dissolution, which is a common diagenetic process in a wide range of geological systems (Weaver 1989; Herrera et al. 2007; Zhang et al. 2007). The purpose of this study is to investigate the evolution of k_0 during mineral dissolution and to identify underlying particle level processes using a combination of experimental and numerical methods.

Experimental Study

Test Device

Various procedures have been devised to measure k_0. In all cases, the radial strain must be kept smaller than $\varepsilon_r < 5 \times 10^{-5}$ to reduce errors in k_0 to less than 0.01 (Okochi and Tatsuoka 1984). Triaxial-type methods involve a flexible lateral boundary and a sensitive feedback system to create the zero lateral deformation condition (Ting et al. 1994). Alternatively a thin wall "soft" oedometer may be designed to permit small lateral deformation to measure the horizontal stress using strain gauges, yet remain within the allowable strain range of $\varepsilon_r < 5 \times 10^{-5}$ to maintain proper k_0 conditions (Kolymbas and Bauer 1993). Soft oedometers have been used to evaluate weathering (Castellanza and Nova 2004) and drying effects on k_0 (Slatter et al. 2005).

The soft oedometer built for this study consists of a thin aluminum shell with an inside diameter of 66 mm and wall thickness of 0.13 mm [Fig. 1(a)]. Porous stones are embedded in the top cap and bottom plate. Deaired water flow is imposed from the bottom of the cell (inlet port) and out through the top cap (outlet port). The nominal specimen height is 40 mm. The vertical settlement of the top cap is measured using a LVDT. Tangential strains are measured using two strain gauges located at the midheight of the specimen (two dummy gauges are included for temperature compensation). The allowable stress level is determined to satisfy the $\varepsilon_r < 5 \times 10^{-5}$ strain criterion. The soft oedometer is calibrated using a water filled balloon inside the cell so that the known vertical stress applied onto the top cap is equal to the horizontal stress; calibration results are shown in Fig. 1(b).

The effects of top and bottom boundary conditions and specimen height on measured tangential strains in the horizontal direction (i.e., strain gauge reading) are numerically evaluated using finite-element simulations. The aluminum cell is modeled as an axisymmetric, linear-elastic material (Young's modulus, $E = 69$ GPa, Poison's ratio, $\nu = 0.3$). The soil pressure against the wall is simulated as either normal stress only (σ_r, $\tau = 0$), or both normal and longitudinal shear stresses (σ_r, $\tau = 0.5 \times \sigma_r$). Furthermore, fixed and free boundary conditions are considered at the bottom of the wall. Simulation results show that top and bottom boundary conditions have minimal effect on the tangential strains measured at midheight when the specimen height to diameter ratio is $H/D \approx 0.6$, while the longitudinal side friction during sediment settlement causes a change in the strain gauge reading smaller than 2%.

Test Procedure

Changes in k_0 during dissolution are investigated using mixtures of glass beads ($d_{50} = 0.7$ mm, spherical shape) and various percentages of table salt ($d_{50} = 0.3$ mm, cubical shape). The two
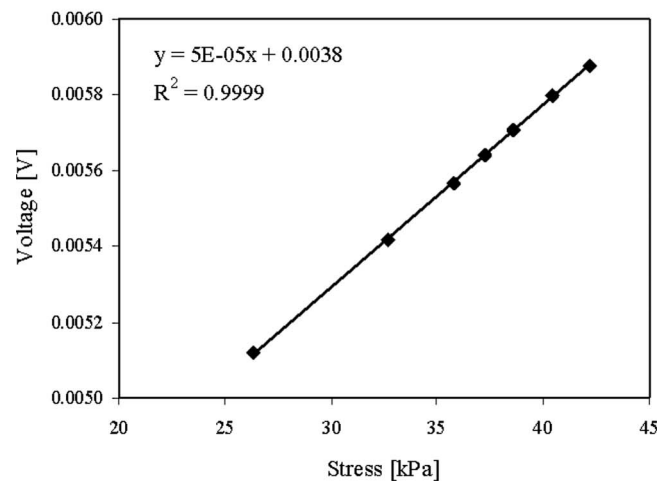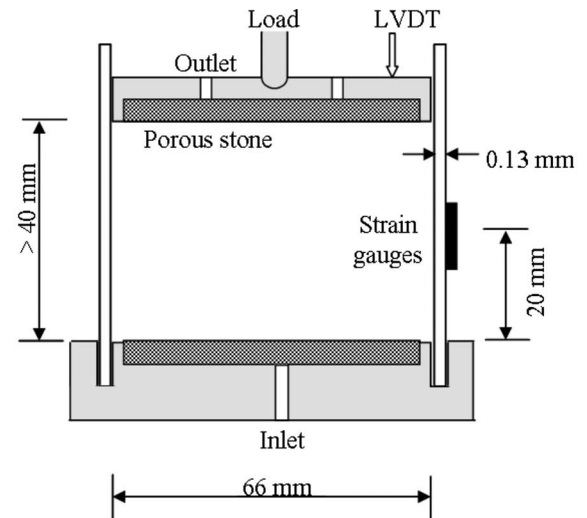

Fig. 1. Device and calibration: (a) soft oedometer; (b) lateral stress calibration

grains are mixed under a salt-saturated brine to prevent dissolution, and scooped into the oedometer cell. The prepared specimen is subjected to vertical loading to 37 kPa. Then, deaired water is allowed from the bottom of the cell to gradually dissolve the salt in the specimen. Water flow is continued until constant specimen height and horizontal stress are reached. When the initial amount of salt is divided by the total volume of water flushed through each specimen, the average concentration is lower than 0.4 mol/L in all tests, which is much lower than the saturation concentration 6 mol/L. Asymptotic stress, stable deformation, and low concentration suggest that full grain dissolution and mass removal was attained in the tests.

Results

The evolution of vertical strain and k_0 are plotted versus time in Fig. 2 for mixtures prepared with a volume of salt divided by the total volume of solids $V_S/V_T = 0$, 5, 10, and 15%. Tests were repeated 2–5 times for each mixture.
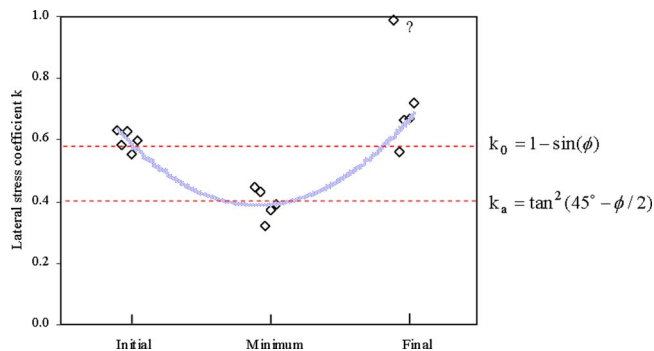
Experimental results show the intricate evolution of k_0. The specimen without salt remains at a constant horizontal stress $k_0 \approx 0.53$ and exhibits no settlement during fluid replacement. All specimens with salt experience a decrease in k_0 during dissolution and reach a minimum value k_{min}. The final k value after dissolu-
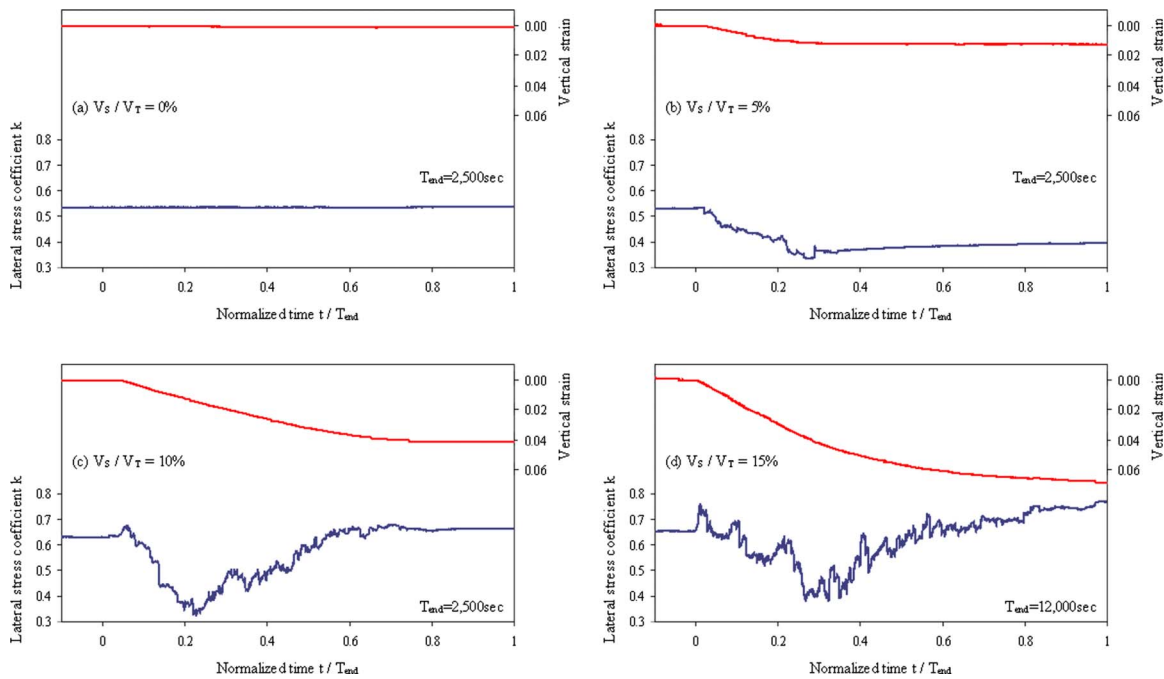
Fig. 2. Dissolution tests—evolution of settlement and lateral stress coefficient k in time. Mixtures with volume fraction of salt V_S/V_T $=V_S/(V_{GB}+V_S)$: (a) 0; (b) 5; (c) 10; and (d) 15% salt.

tion is lower than the initial value before dissolution in specimens with 5% salt fraction. However, specimens with 10 and 15% salt fraction exhibit multiple oscillations in k_0; eventually, the horizontal stress recovers from the minimum k_{min} to end near the initial value k_0 when dissolution ends.

Results for five similar specimens prepared with 10% salt are summarized in Fig. 3. As observed above, there is pronounced variability in the minimum and final stress ratios k. Jaky's equation $k_0=1-\sin(\phi)$ and Rankine's active coefficient equation k_a $=\tan^2(45°-\phi/2)$ are computed using the friction angle determined from the angle of repose method (as in Santamarina and Cho 2001): the measured angle of repose for the glass beads is $\phi=25\pm0.5°$ and it is not affected by the presence of soluble salt for $V_S/V_T\leq25\%$. Computed values are superimposed on Fig. 3.

The estimated k_0 matched the initial and final values, while the measured k_{min} is in the range of the active earth pressure coefficient k_a.

The measured settlement is normalized by the initial specimen height and plotted versus the volume fraction of salt in Fig. 4. The measured vertical strain is much lower than the volume fraction of dissolved particles.
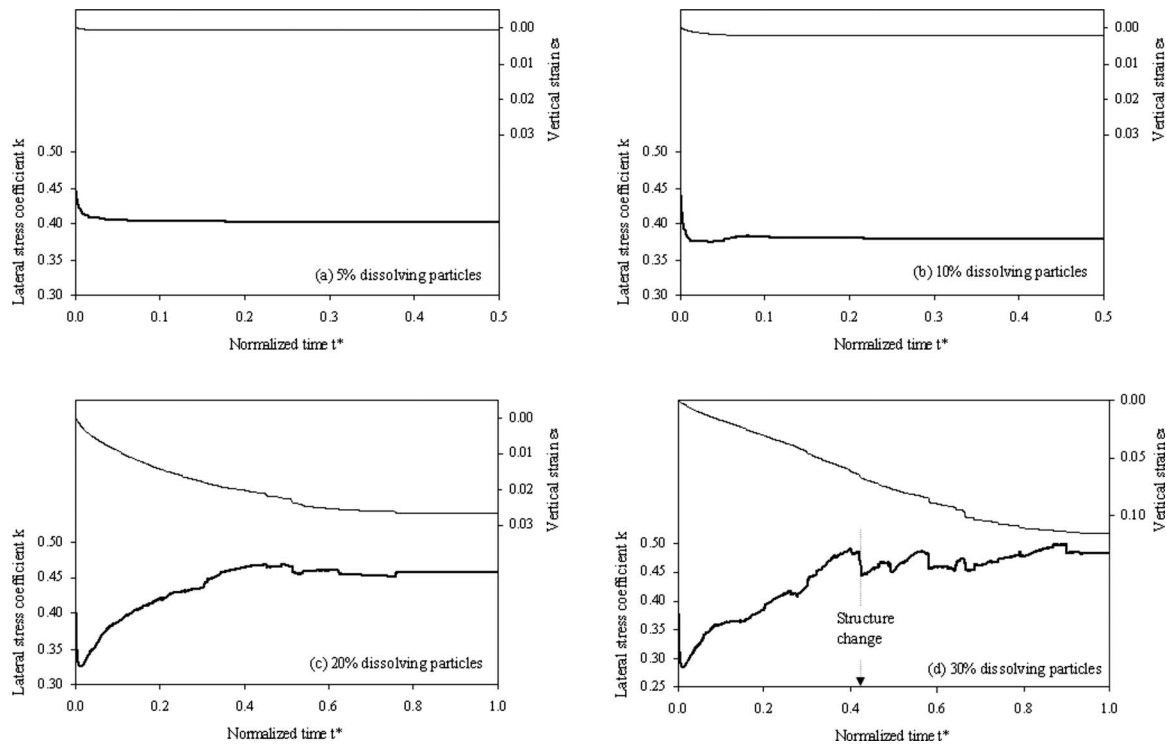

Fig. 3. Variation of lateral stress coefficient k during dissolution. Set of five tests run on similar specimens made of $V_S/V_T=10\%$. Lateral stress coefficient before, during, and after dissolution. Estimated Jaky's k_0 and Rankine's k_a are shown for mixture friction angle of $\phi=25°$.
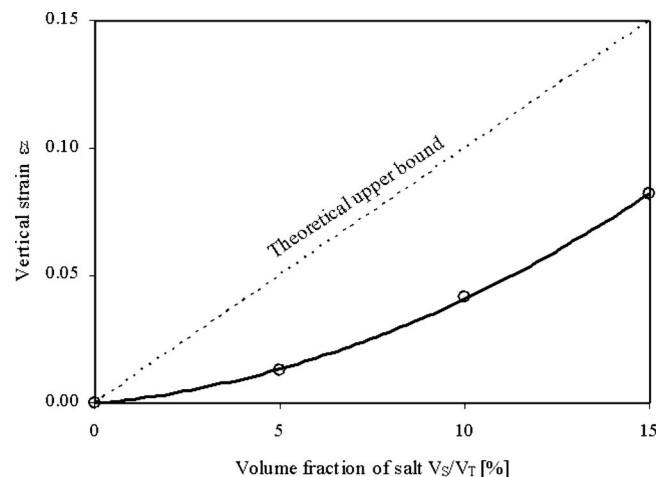
Fig. 4. Experimentally determined vertical strain at end of dissolution as function of volume of dissolving particles, V_S/V_T. Theoretical upper bound is estimated assuming that void ratio is same before and after dissolution.

Fig. 5. DEM simulation. Evolution of settlement and lateral stress coefficient during particle dissolution. Normalized time t^* is current time step divided by time at 100% dissolution. Volume fraction of dissolving particles V_S/V_T: (a) 5; (b) 10; (c) 20; and (d) 30%. Simulation conditions: interparticle friction $\mu=0.5$, standard deviation in particle radius 25%, hindered particle rotation.

## Discrete Element Simulations

Methodology

The discrete element method is used to gain particle level insight into the consequences of mineral dissolution. The two-dimensional (2D) simulation involves 9,999 disks with 25% standard deviation in particle size (PFC-2D, Itasca). The packing is subjected to vertical confinement under zero lateral strain and no friction is assumed between particles and walls $[\sigma_z/K_n=10^{-3}$, where K_n (N/m^2) is normal contact stiffness]. Then a servo-control function is used to maintain the vertical stress constant during dissolution. Simulations are repeated for the following volume fraction of particles subjected to contraction: 5, 10, 15, 20, 30, 40, and 50%. Dissolution is simulated by decreasing the particle size (Note: preliminary simulations were conducted by reducing the shear modulus and produced similar trends).
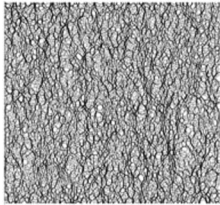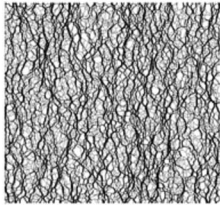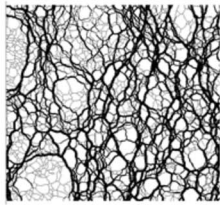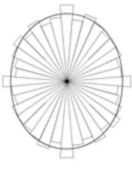
Results

Typical simulation results are summarized in Fig. 5. The following observations can be made: (1) general trends agree with experimental results presented in Fig. 2; (2) dissolution causes vertical settlement and an early decrease in horizontal stress; (3) the final k is lower than the initial k_0 in tests with less than 15% dissolving particles and both settlement and horizontal stress stabilize at an early stage; (4) horizontal stress recovery takes place when the volume fraction of dissolving particles exceeds 15%; and (5) both experimental (Fig. 2) and numerical (Fig. 5) results show quite s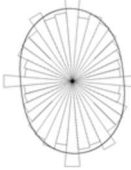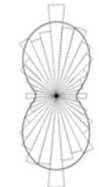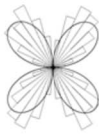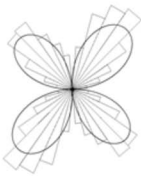mooth vertical settlement in all cases, while rough changes in horizontal stress take place in large V_S/V_T specimens.

The changes in the anisotropy of internal parameters is recorded in all simulations: a_c captures contact anisotropy (1

$+a_c \cos 2\theta$), a_n normal force anisotropy $(1+a_n \cos 2\theta)$, and a_t shear force anisotropy $(a_t \sin 2\theta)$. Fig. 6 shows the evolution of each parameter for the simulation with a 20% volume fraction of
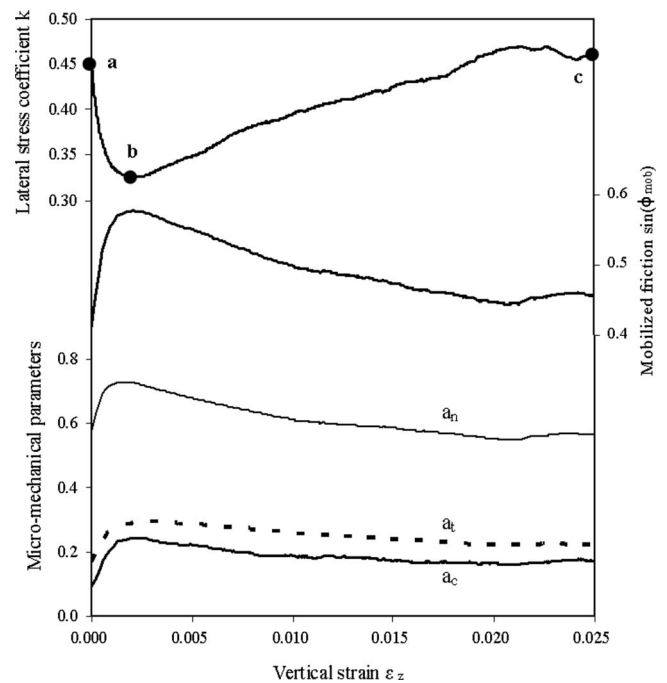
Fig. 6. DEM simulation. Evolution of horizontal stress coefficient, mobilized friction sin ϕ_{mob}, and micromechanical parameters during dissolution. Simulation conditions: interparticle friction $\mu=0.5$, hindered particle rotation, volume fraction of dissolving particles 20%.

Stages in Fig. 6	(a)	(b)	(c)
	Before dissolution	During dissolution at k minimum	After dissolution
Chains of contact normal forces			
Number of contacts			
Average normal contact forces			
Average tangential contact forces			
k	0.45	0.33	0.46
$\sin(\phi_{mob})$	0.41	0.58	0.46
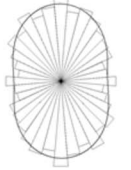
Fig. 7. DEM simulation; fabric and polar plots of internal micromechanical parameters before, during, and after dissolution—refer to Fig. 6 for Stages a, b, and c (20% volume fraction of dissolving particles)

dissolving particles. Anisotropy is most pronounced in normal contact forces a_n. The three parameters a_c, a_n, and a_t reach a peak in anisotropy as the medium approaches the minimum value in the lateral stress coefficient.

Fig. 7 shows statistical summaries of micromechanical parameters in the form of polar plots at the initial state ("a" in Fig. 6), at the minimum horizontal stress during dissolution ("b" in Fig. 6), and at the final state after dissolution ("c" in Fig. 6) for the simulation with 20% volume fraction of dissolving particles. The polar plots confirm the increased anisotropy in contacts, normal and shear forces reported in Fig. 6. Furthermore, profound differences in fabric are observed between the initial and the final stages (not detected in statistical summaries): marked force chains, a "honeycomb fabric," and force arches characterize the fabric after dissolution. Therefore, while the stress ratio k is similar before and after dissolution in this simulation (Fig. 6), the internal fabric is distinct and a different sediment response is anticipated upon further loading.

Fig. 8 shows the final settlement obtained in the simulations with different volume fractions of dissolving particles. Analogous
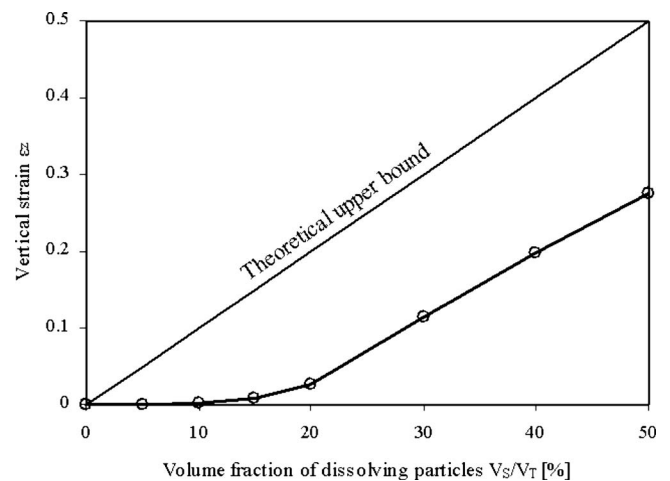
Fig. 8. DEM simulation; vertical strain at end of dissolution as function of volume fraction of dissolving particles V_S/V_T. Theoretical upper bound presumes that void ratio is same before and after dissolution.

to experimental data (Fig. 4), strains are small for low V_S/V_T ratios, but increase significantly thereafter (for $V_S/V_T=20\%$ in these 2D simulations).

Discussion

Vertical Settlement during Dissolution

Assuming the same void ratio before and after dissolution, the strain due to dissolution would be (Note: very loose materials could densify during dissolution)

$$\varepsilon_z = \frac{1}{1 + G_S M_{GB}/G_{GB}M_S} = \frac{V_S}{V_T} \quad (3)$$

where subscripts GB and S denote "glass bead" and dissolving granular "salt" respectively; V_S=volume of salt; and V_T=initial total volume of solids. The predicted strain is superimposed on experimental and numerical results in Figs. 4 and 8. The measured strains are much smaller than the strain estimated using Eq. (3); this is in agreement with the development of load carrying grain arches around the dissolving particles and the increase in internal porosity loading to the honeycomb fabric. In particular, the final vertical strain ε_z is small at low V_S/V_T ratios, however strains track grain dissolution at high volume fractions above a certain V_S/V_T threshold. Therefore, it appears that a limiting porosity or "terminal density" is reached during dissolution so that further dissolution must be accompanied by volume collapse. The V_S/V_T threshold is higher in the 2D simulations ($V_S/V_T \approx 20\%$) than in the 3D experimental results ($V_S/V_T \approx 10\%$), probably due to inherent differences in particle mobility in 2D and 3D systems.

Stiffness Evolution

Q. H. Truong, Y. H. Eom, and J. S. Lee ("Stiffness characteristics of vanishing mixtures," unpublished, 2009) conducted complementary tests using mixtures of silica sand and soluble salt to study the evolution of stiffness during dissolution. They observed a marked decrease in shear wave velocity and small strain shear modulus during particle dissolution; furthermore, they found that stiffness does not recover to the before-dissolution trend but remains low upon further k_0 loading. These results agree with the reduction in lateral stress (transient in high V_S/V_T mixtures) and the higher final void ratio (all mixtures) observed in our experiments and numerical simulations.

Smooth Settlement and Episodic k Changes

Both experimental and numerical results show that vertical settlement evolves smoothly during particle dissolution, while the measured horizontal stress shows more dramatic episodic changes (see Figs. 2 and 5). While stick-slip behavior between wall and ductile grains can produce oscillation in vertical stress measurements during self-weight deformation ($H/D=1-4$ and $D/d=3.4-7.6$) (Uri et al. 2006), a smooth settlement response is observed in all our experiments suggesting minimal side wall friction effects on both settlement and horizontal stress measurements (in agreement with the low H/D ratio used in this study) (Ovarlez and Clement 2003). Therefore, an alternative explanation is sought herein.

Insight is gained by studying the changes in internal anisotropy parameters: the granular fabric must be continuously evolving to sustain the applied vertical stress while grain dissolution
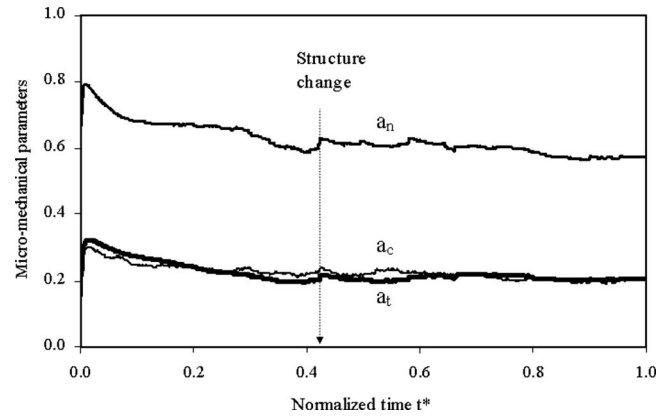
Fig. 9. DEM simulation; evolution of micromechanical parameters during dissolution. Corresponding trends for settlement and lateral stress coefficient k are shown in Fig. 5(d). Notice jump in k at t^* =0.42 in Fig. 5(d) and corresponding structure change in this figure. Simulation conditions: interparticle friction μ=0.5, volume fraction of dissolving particles 30%.

takes place. Indeed, Fig. 9 shows that sudden increases in micromechanical anisotropy parameters a_n, a_t, and a_c accompany the episodic k [drops [Fig. 5(d)]. Hence, dissolution causes local fabric changes and pronounced changes in force transmission that have an immediate effect on k but a delayed integration into global settlement.

Mobilized Friction

The anisotropy in internal parameters can be used to estimate the mobilized shear strength within the particulate medium (Rothenburg and Bathurst 1989)

$$\sin(\phi_{mob}) = \frac{1/2(a_c + a_n + a_t)}{1 + a_c a_n/2} \quad (4)$$

The evolution in mobilized friction during dissolution is superimposed on the plot for horizontal stress change in Fig. 6. Results show that k_0 reaches the minimum value when the mobilized friction angle is maximum. The mobilized friction ϕ_{mob} confirms that internal shear failure conditions may be reached during dissolution.

Macroscale Effects

It can be shown following Rudnicki and Rice (1975) that shear localization may take place during mineral dissolution in sediments that exhibit postpeak strain softening (details in Shin et al. 2008). This could explain the formation of polygonal fault systems observed in offshore basins worldwide (Cartwright and Dewhurst 1998), as well as the development of internal shear planes in volcanic ash soils which evolved onshore from the in situ dissolution of wind transported volcanic ash (Herrera et al. 2007).

Conclusions

The in-situ state of stress under zero lateral strain conditions, captured in the k_0 parameter, is a complex consequence of sediment properties and the formation history of natural sediments. Empirical equations fail to capture the effects of formation his-

tory, and there is limited information related to the postdepositional evolution of k_0 during soil diagenesis in particular as a consequence of mineral dissolution. Experiments and discrete element numerical simulations reported in this paper help gain insight into the effect of mineral dissolution on internal stress and deformation.

Mineral dissolution under zero lateral strain and constant vertical stress results in horizontal stress decrease. The minimum horizontal stress coefficient k_{min} can be as low as Rankine's active earth pressure coefficient. Discrete element simulation results confirm that the internal friction is fully mobilized at k_{min}. Hence, internal shear failure can be reached during grain dissolution.

A small amount of dissolving particles is sufficient to trigger the horizontal stress drop. If the volume of dissolving particles V_S/V_T is small, there is no stress recovery and the change in void ratio is very minor. Once a threshold value V_S/V_T is exceeded, the horizontal stress recovers, a low terminal density is reached, and the vertical strain increases proportionally to the amount of dissolving particles.

Mineral dissolution involves rearrangement of the internal granular structure. While the lateral stress coefficient may be similar before and after dissolution (i.e., a medium with V_S/V_T above the threshold value), the internal fabric is quite distinct and it is characterized by a honeycomb structure with pronounced force chain arching.

Acknowledgments

References

Abdelhamid, M. S., and Krizek, R. J. (1976). "At rest lateral earth pressure of a consolidating clay." *J. Geotech. Engrg. Div.*, 102(7), 721–738.

Andrawes, K. Z., and El-Sohby, M. A. (1973). "Factors affecting coefficient of earth pressure k_0." *J. Soil Mech. and Found. Div.*, 99(7), 527–539.

Berre, T., Tunbridge, L., and Hoeg, K. (1995). "The measurement of small strains and the k_0 value in triaxial tests on clay-shales." *Proc., 8th Int. Cong. Rock Mechanics*, Taylor & Francis, Tokyo, Vol. 3, 1195–1199.

Bishop, A. W., and Eldin, A. K. G. (1953). "The effect of stress history on the relation between φ and porosity in sand." *Proc., 3rd Int. Conf. on Soil Mechanics and Foundation Engineering*, Zurich, Vol. 1, 100–105.

Brooker, E. W., and Ireland, H. O. (1965). "Earth pressures at rest related to stress history." *Can. Geotech. J.*, 2(1), 1–15.

Cartwright, J. A., and Dewhurst, D. N. (1998). "Layer-bound compaction faults in fine-grained sediments." *Geol. Soc. Am. Bull.*, 110(10), 1242–1257.

Castellanza, R., and Nova, R. (2004). "Oedometric tests on artificially weathered carbonatic soft rocks." *J. Geotech. Geoenviron. Eng.*, 130(7), 728–739.

Feda, J. (1984). "k_0 coefficient of sand in triaxial apparatus." *J. Geotech. Engrg.*, 110(4), 519–524.

Herrera, M. C., Lizcano, A., and Santamarina, J. C. (2007). "Colombian volcanic ash soils." *Characterization and engineering properties of natural soils*, Taylor & Francis, Singapore, 2385–2409.

Holtz, R. D., and Jamiolkowski, M. B. (1985). "Discussion of 'Time

dependence of lateral earth pressure.'" *J. Geotech. Engrg.*, 111(10), 1239–1242.

Jaky, J. (1944). "The coefficient of earth pressure at rest." *J. for Society of Hungarian Architects and Engineers*, 78(22), 355–358 (in Hungarian).

Jamiolkowski, M., Ladd, C. C., Germaine, J. T., and Lancellotta, R. (1985). "New developments in field and laboratory testing of soils." *Proc., 11th Int. Conf. on Soil Mechanics and Foundation Engineering*, San Francisco, Vol. 1, 57–154.

Kavazanjian, E., Jr., and Mitchell, J. K. (1984). "Time dependence of lateral earth pressure." *J. Geotech. Engrg.*, 110(4), 530–533.

Kolymbas, D., and Bauer, E. (1993). "Soft oedometer. A new testing device and its application for the calibration of hypoplastic constitutive laws." *Geotech. Test. J.*, 16(2), 263–270.

Kulhawy, F. H., and Mayne, P. W. (1990). *Manual on estimating soil properties for foundation design*, Electric Power Research Institute, Palo Alto, Calif.

Mayne, P. W., and Kulhawy, F. H. (1982). "k_0-OCR relationships in soil." *J. Geotech. Engrg. Div.*, 108(6), 851–872.

Mesri, G., and Hayat, T. M. (1993). "Coefficient of earth pressure at rest." *Can. Geotech. J.*, 30(4), 647–666.

Michalowski, R. L. (2005). "Coefficient of earth pressure at rest." *J. Geotech. Geoenviron. Eng.*, 131(11), 1429–1433.

Muir Wood, D. (1990). *Soil behaviour and critical state soil mechanics*, Cambridge University Press, Cambridge, U.K.

Okochi, Y., and Tatsuoka, F. (1984). "Some factors affecting k_0 values of sand measured in triaxial cell." *Soils Found.*, 24(3), 52–68.

Ovarlez, G., and Clement, E. (2003). "Slow dynamics and aging of a confined granular flow." *Phys. Rev. E*, 68(3), 031302.

Roscoe, K. H., and Burland, J. B. (1968). "On the generalized stress-strain behaviour of 'wet' clay." *Engineering plasticity*, J. Heyman and F. A. Leckie, eds., Cambridge University Press, Cambridge, U.K., 535–609.

Rothenburg, L., and Bathurst, R. J. (1989). "Analytical study of induced anisotropy in idealized granular materials." *Geotechnique*, 39(4), 601–614.

Rudnicki, J. W., and Rice, J. R. (1975). "Conditions for the localization of deformation in pressure-sensitive dilatant materials." *J. Mech. Phys. Solids*, 23(6), 371–394.

Santamarina, J. C., and Cho, G. C. (2001). "Determination of critical state parameters in sandy soils—Simple procedure." *Geotech. Test. J.*, 24(2), 185–192.

Schmertmann, J. H. (1983). "A simple question about consolidation." *J. Geotech. Engrg.*, 109(1), 119–122.

Shin, H., Santamarina, J. C., and Cartwright, J. A. (2008). "Contraction-driven shear failure in compacting uncemented sediments." *Geology*, 36(12), 931–934.

Skempton, A. W. (1961). "Horizontal stresses in an overconsolidated Eocene clay." *Proc., 5th Int. Conf. Soil Mechanics Foundation Engineering*, Paris, Vol. 1, 351–357.

Slatter, E. E., Fityus, S. G., and Smith, D. W. (2005). "Measuring lateral pressures during suction controlled one dimensional consolidation." *Proc., Int. Symp. on Advanced Experimental Unsaturated Soil Mechanics*, Taylor & Francis, London, Trento, Italy, 117–124.

Ting, C. M. R., Sills, G. C., and Wijeyesekera, D. C. (1994). "Development of k_0 in soft soils." *Geotechnique*, 44(1), 101–109.

Uri, L., Dysthe, D. K., and Feder, J. (2006). "Oscillatory ductile compaction dynamics in a cylinder." *Phys. Rev. E*, 74(3), 031301.

Weaver, C. E. (1989). *Clays, muds, and shales*, Elsevier, Amsterdam, The Netherlands.

Zhang, G., Whittle, A. J., Germaine, J. T., and Nikolinakou, M. A. (2007). "Characterization and engineering properties of the old alluvium in Puerto Rico." *Characterization and engineering properties of natural soils*, Taylor & Francis, Singapore, 2557–2588.

Zhu, F., Clark, J. I., and Paulin, M. J. (1995). "Factors affecting at-rest lateral stress in artificially cemented sands." *Can. Geotech. J.*, 32(2), 195–203.